Supplementary Information

FTO-Mediated Formation of N^6-Hydroxymethyladenosine and N^6-Formyladenosine in Mammalian RNA

Ye Fu[1,*], Guifang Jia[1,*], Xueqin Pang[2,3], Richard N. Wang[1], Xiao Wang[1], Charles J. Li[1], Scott Smemo[4], Qing Dai[1], Kathleen A. Bailey[4], Marcelo A. Nobrega[4], Ke-li Han[3], Qiang Cui[2], Chuan He[1]

[1]Department of Chemistry and Institute for Biophysical Dynamics, The University of Chicago, 929 East 57th Street, Chicago, IL 60637, USA. [2]Department of Chemistry and Theoretical Chemistry Institute, University of Wisconsin, Madison, WI 53706, USA. [3]Dalian Institute of Chemical Physics, Chinese Academy of Sciences, Dalian, Liaoning, 116023, PR China. [4]Department of Human Genetics, The University of Chicago, 920 E. 58th Street, Chicago, IL 60637, USA. [*]These authors contributed equally to the work. Correspondence and requests for materials should be addressed to C.H. (email: chuanhe@uchicago.edu).

Content

Supplementary Figure S1 to Supplementary Figure S25	S2-S26
Supplementary Table S1	S27
Supplementary Methods	S28-S31
Synthesis of N^6-hydroxymethyladenosine (hm^6A)	S28
Synthesis of N^6-formyladenosine (f^6A)	S28
EMSA of Modified RNA with YTHDF2 Protein	S28
Two Independent Protocols for Setting up the FTO-Base Systems	S29
MD Simulation Setup	S29
Alchemical Free Energy Simulations for Relative Binding Affinities	S30
YTHDF2 Nucleotide Sequence	S30
Supplementary References	S31

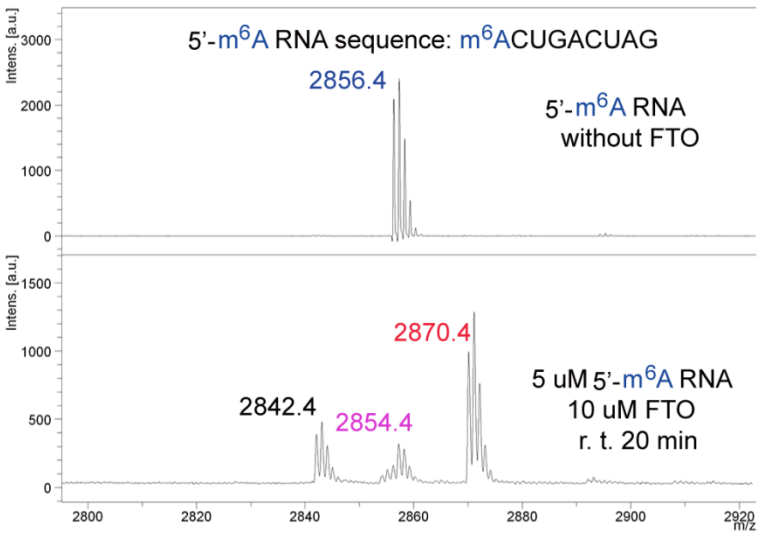

Supplementary Figure S1. MALDI-TOF analysis shows FTO possesses similar activity on RNA oligo with terminal m^6A and internal m^6A. RNA oligo with 5'-m^6A was treated with FTO in the same manner as internal m^6A, similar activity was observed when compared with RNA oligo with internal m^6A (Fig. 1b).

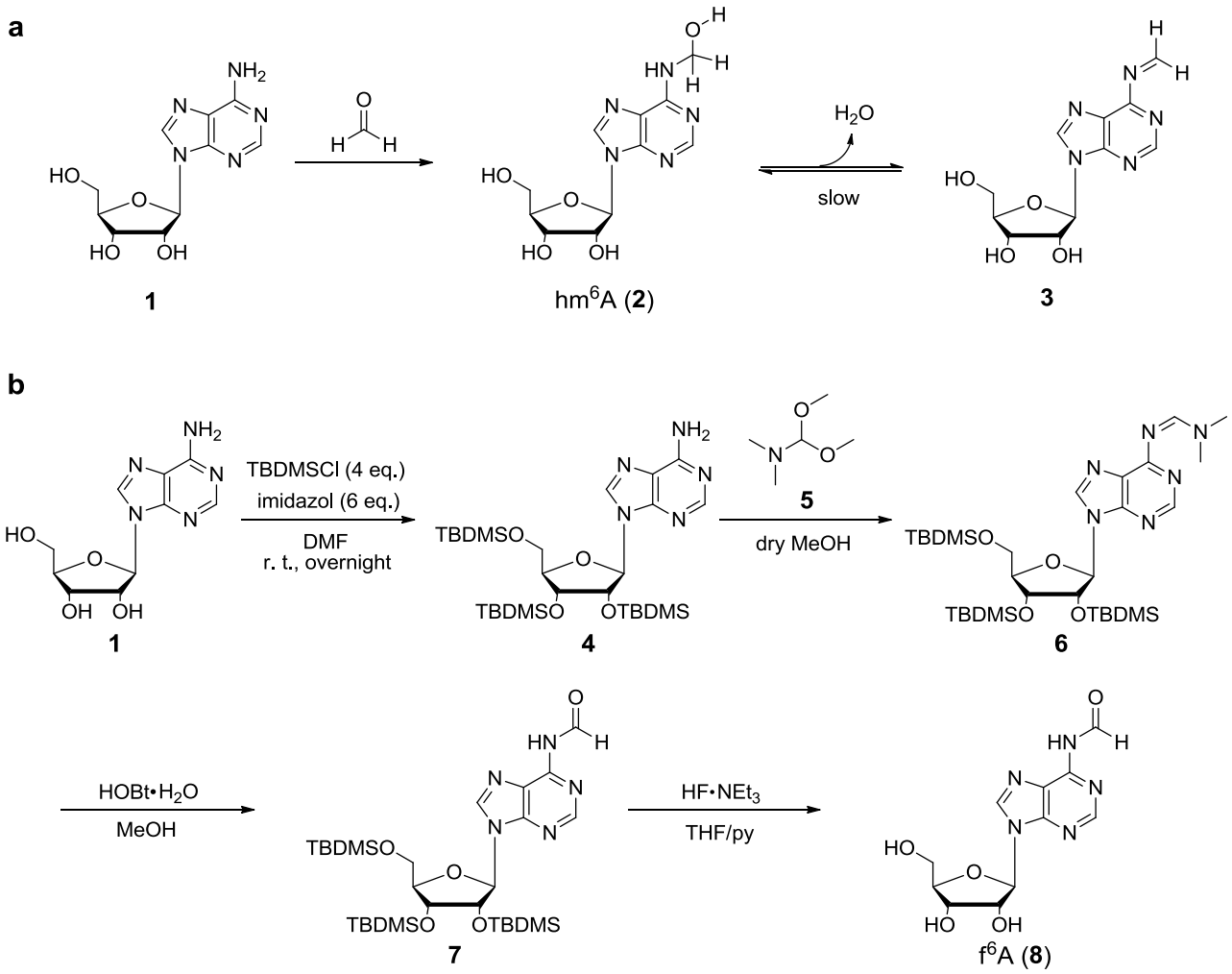

Supplementary Figure S2. Syntheses of hm^{6}A and f^{6}A standards. (**a**) 100 uM of adenosine (**1**) was treated with 30 mM of formaldehyde at 60 ºC for 4 hrs to produce hm^{6}A (**2**), which partially dehydrated to *N*^{6}-methylene-adenosine (**3**) in equilibrium. (**b**) Adenosine (**1**) was first protected with TBDMS (**2**) using TBDMSCl, and *N*,*N*-dimethylformamidine (**6**) using dimethyl acetal *N*,*N*-dimethylformamide (**5**). **6** was treated with weak acid *N*-hydroxybenzotriazole (HOBt·H_2O) in MeOH to generate TBDMS-protected f^{6}A (**7**). Deprotection of the TBDMS protecting group using HF·NEt_3 yielded f^{6}A (**8**) as the final product.

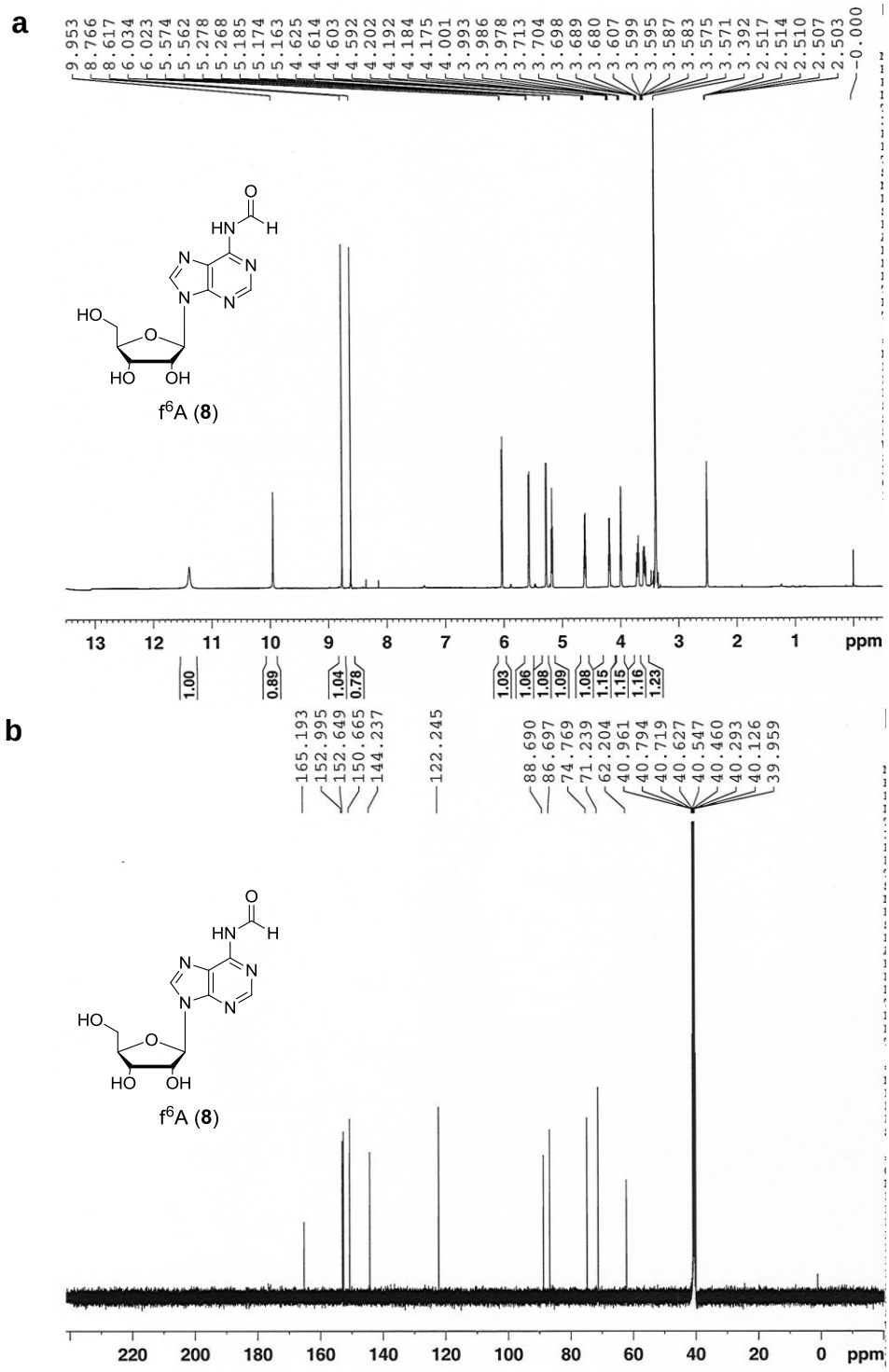

Supplementary Figure S3. ^{1}H (a) and ^{13}C (b) NMR spectra of f^{6}A (8) standard.

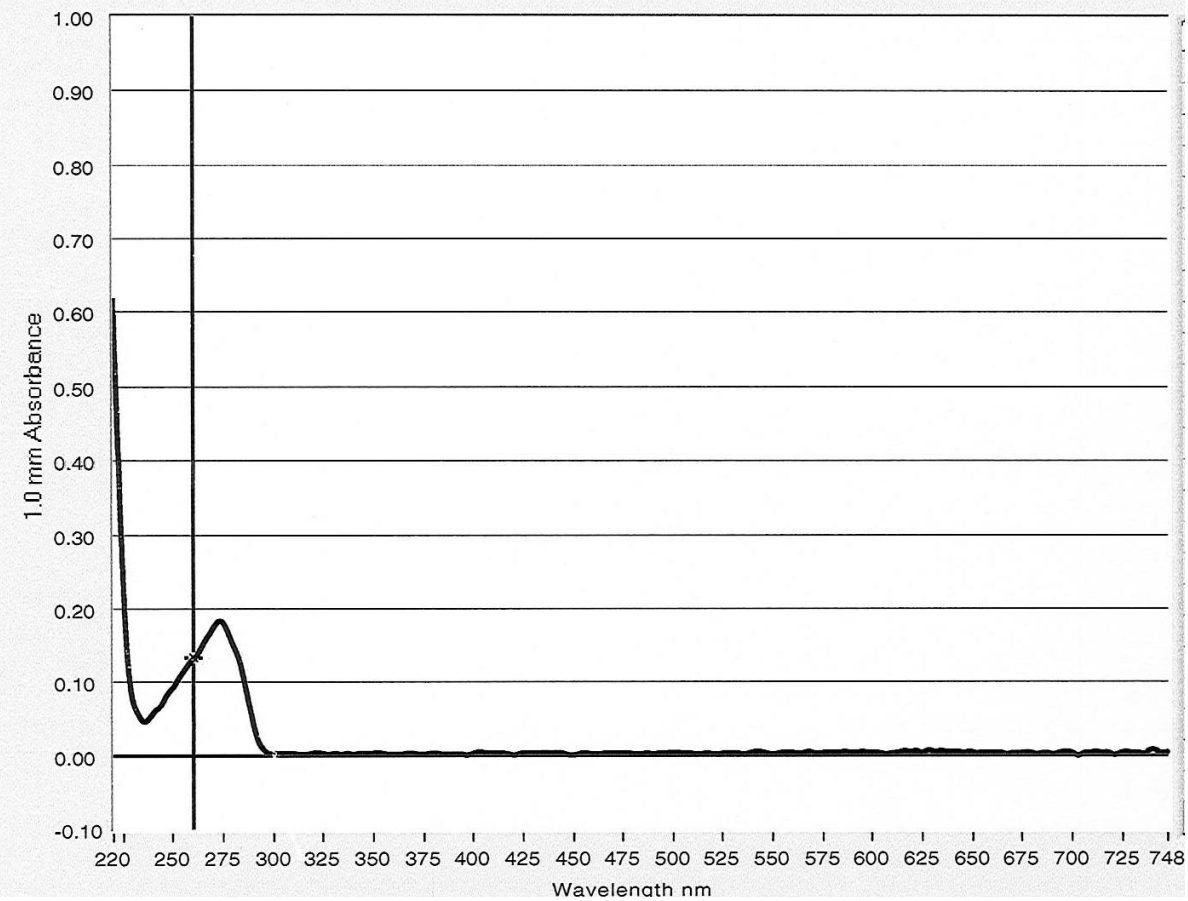

Supplementary Figure S4. UV-Vis absorption spectra of f^{6}A (8) standard in 100 uM solution in water.

$\varepsilon_{260nm}=1.30\times10^{4}\ M^{-1}cm^{-1}$

$\varepsilon_{max(274nm)}=1.83\times10^{4}\ M^{-1}cm^{-1}$

a

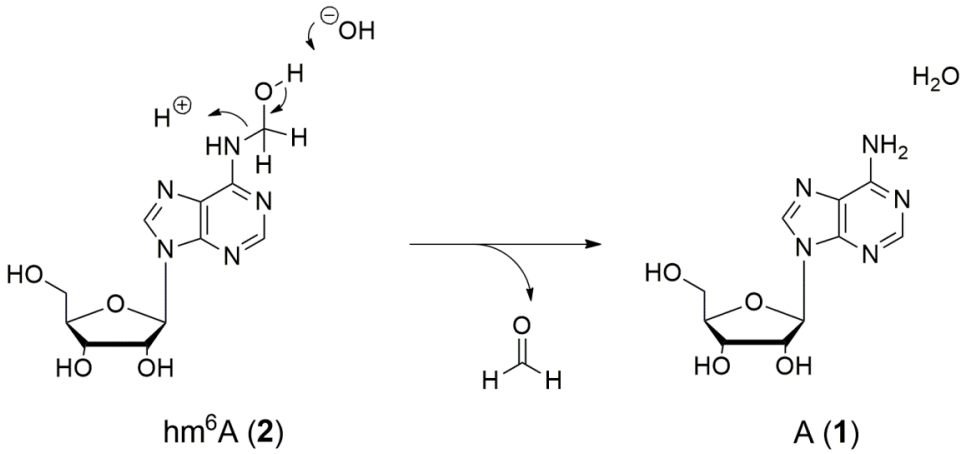

hm^{6}A (**2**) A (**1**)

b

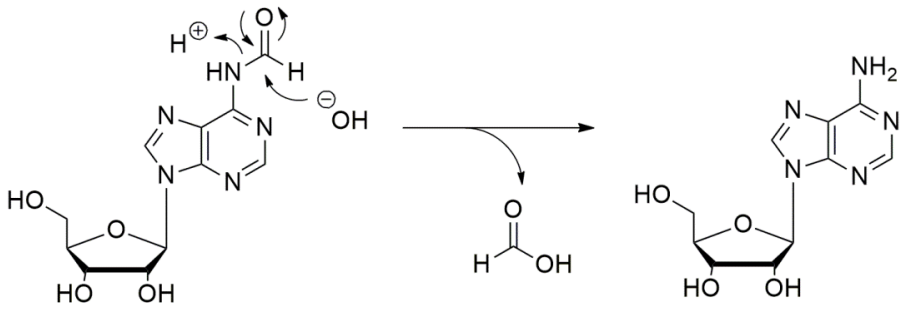

f^{6}A (**8**) A (**1**)

Supplementary Figure S5. Spontaneous hydrolysis of hm^{6}A (2) and f^{6}A (8) in water. Hydrolysis of hm^{6}A (**a**) and f^{6}A (**b**) in water, which are accecelarated in both acidic and basic conditions.

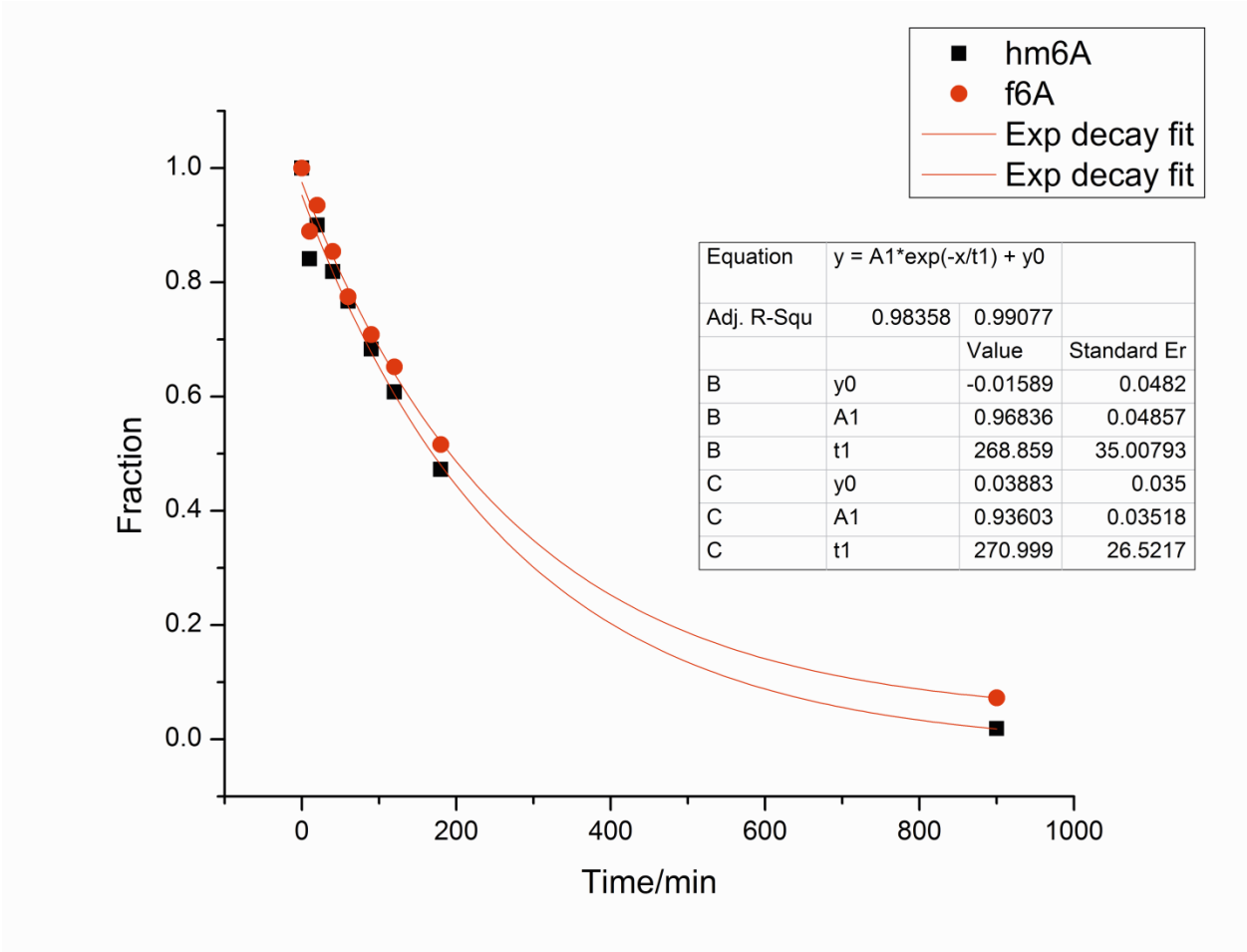

Equation	y = A1*exp(-x/t1) + y0		
Adj. R-Squ	0.98358	0.99077	
		Value	Standard Er
B	y0	-0.01589	0.0482
B	A1	0.96836	0.04857
B	t1	268.859	35.00793
C	y0	0.03883	0.035
C	A1	0.93603	0.03518
C	t1	270.999	26.5217

Supplementary Figure S6. Hydrolysis of hm^{6}A (2) and f^{6}A (8) in buffer at 37 °C. $T_{1/2}$ = 186±25 min for hm^{6}A, $T_{1/2}$ = 188±18 min for f^{6}A. 0.5 nmol of RNA containing 5' m^{6}A is treated with 50 mol% of FTO in 50 uL of solution, followed by Nuclease P1 digestion to generate hm^{6}A and f^{6}A *in situ*. The solution is then diluted 10 times into buffer containing 20 mM of Tris-HCl pH 7.4, 140 mM of KCl, 15 mM of NaCl, and 1mM of $MgCl_2$.The solution is further diluted 10 times in H_2O before injected into HPLC-QQQ-MS/MS for quantification. The decay curve is fitted into a expontential decay function, $T_{1/2}$ is calculated by multiplying the fitted t1 with ln2.

a

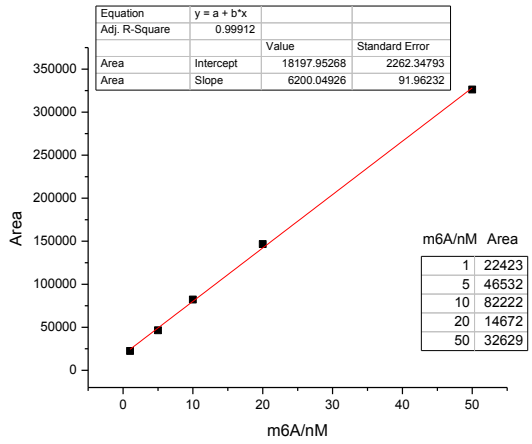

b

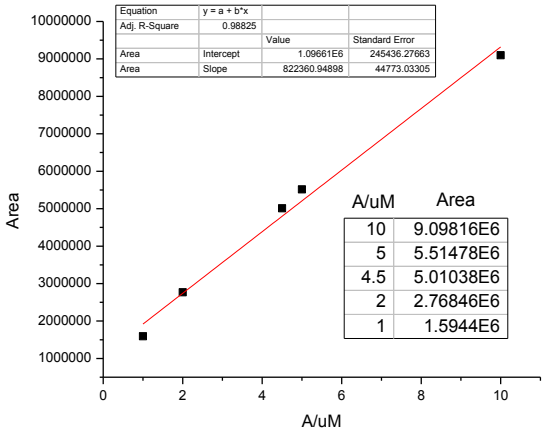

c

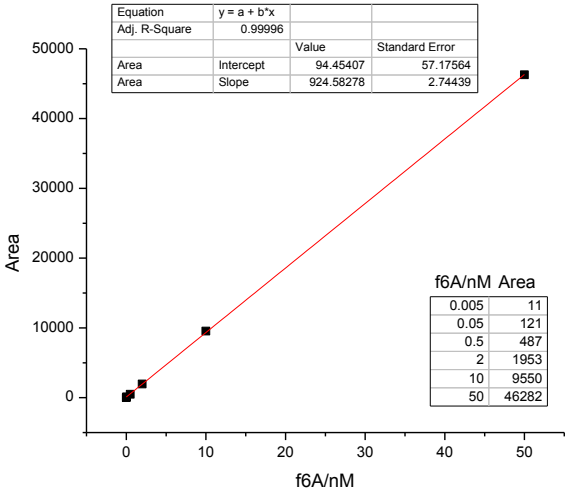

Supplementary Figure S7. Quantification standard curve of m^6A (a), A (b) and f^6A (c) standards in HPLC-QQQ-MS/MS.

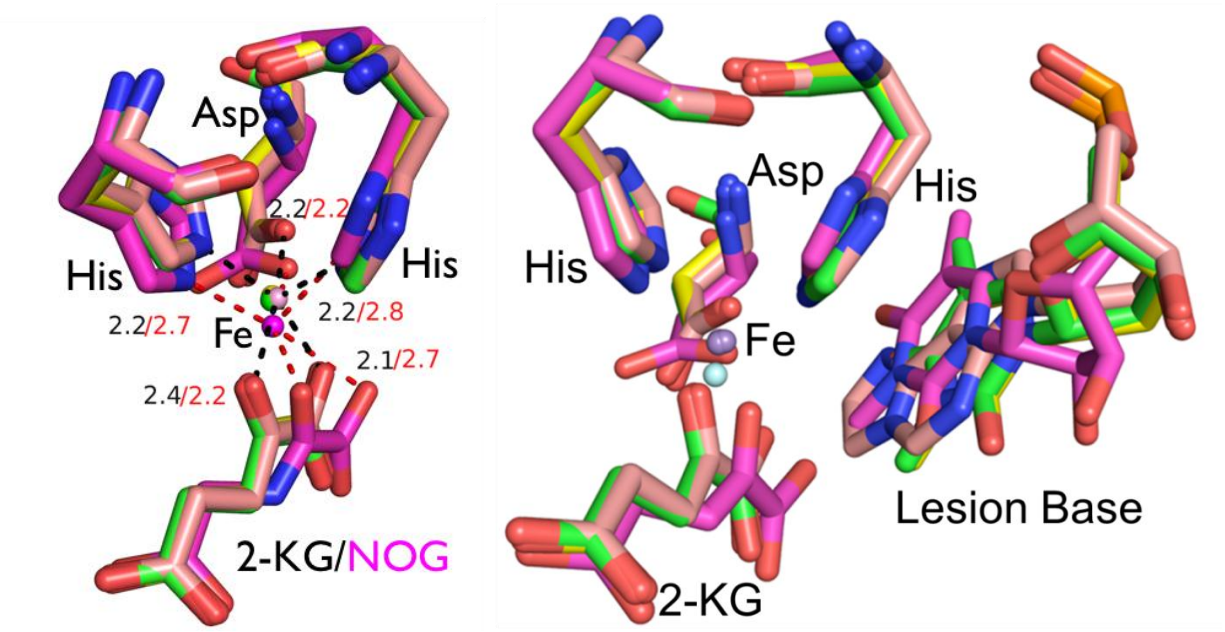

Supplementary Figure S8. Overlap of FTO and AlkB active site. Active site geometry comparison between FTO and AlkB.FTO-m^3T, PDB ID: 3LFM; AlkB-m^3C, PDB ID: 3O1M; AlkB-m^3T, PDB ID: 3O1O; AlkB-εA, PDB ID: 3O1P.The distances between Fe^{2+} and its coordinating ligands in the active site of FTO are systematically larger than those in AlkB, due most likely to the antagonist binding and lower resolution of the FTO crystal structure.

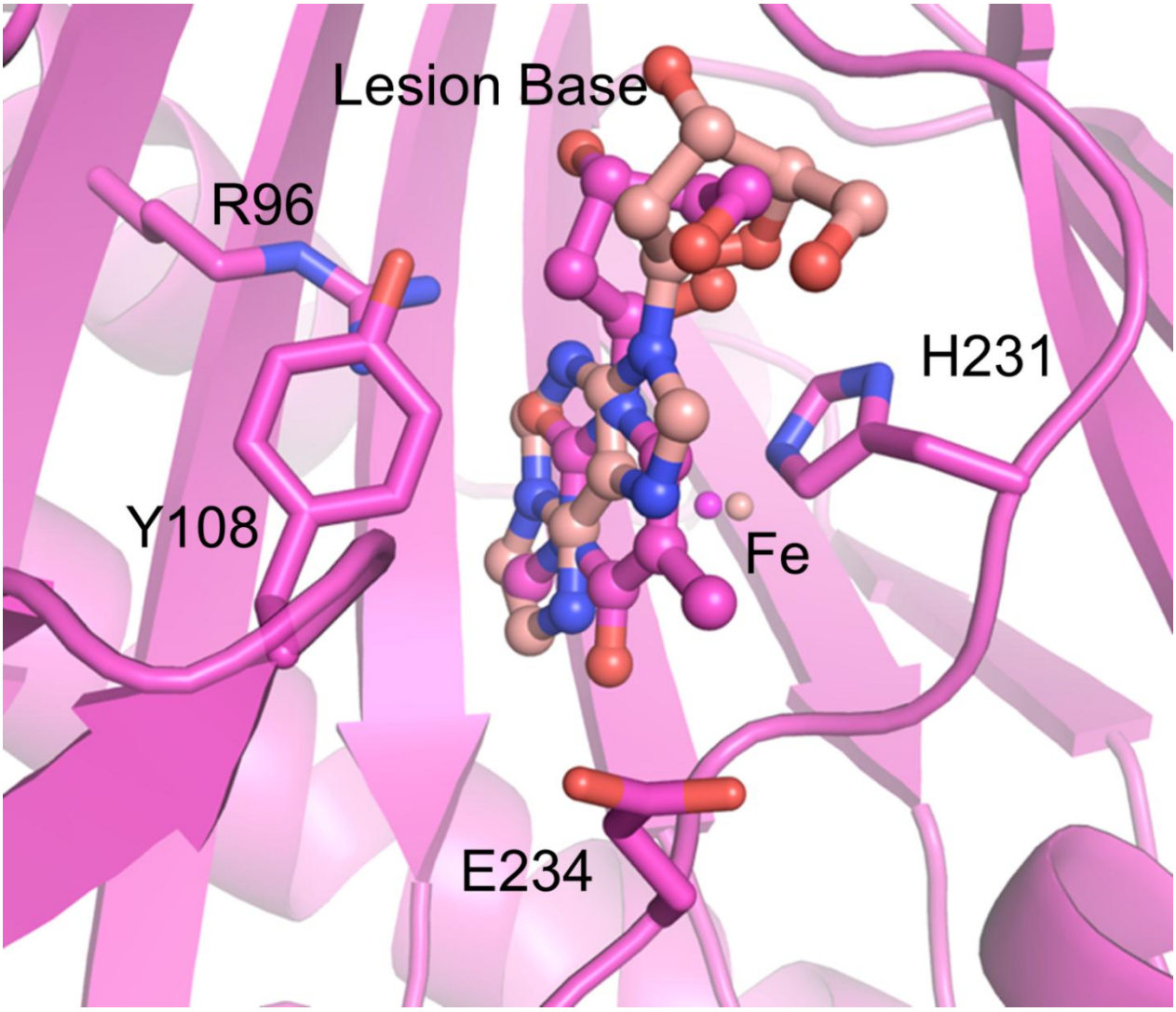

Supplementary Figure S9. Comparison of modified base binding mode in FTO/AlkB (3lfm-m^3T/3o1p-εA). Similar position of targeting Carbon atoms is observed.

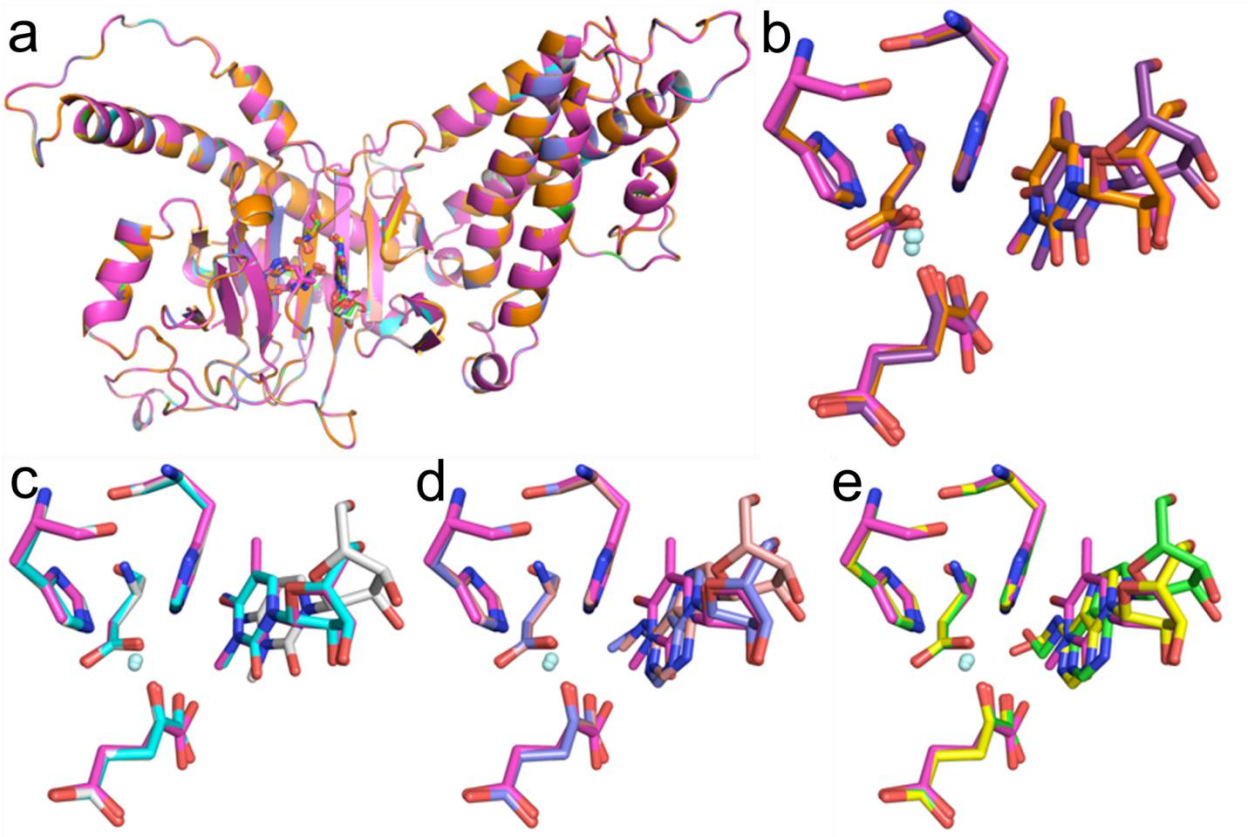

Supplementary Figure S10. Structure comparison after minimization. (**a**) Global-view with the protein structure shown in cartoon and active site residues in sticks. (**b**) FTO-m^3T-cry/FTO-m^3T-alkb (**c**) FTO-m^3C-cry/FTO-m^3C-alkb (**d**) FTO-m^6A-cry/FTO-m^6A-alkb (**e**) FTO-hm^6A-cry/FTO-hm^6A-alkb (FTO crystal structure)("cry" uses base coordinates from FTO-m^3T crystal structure, "alkb" uses base coordinates from aligned AlkB-DNA complex structures.)

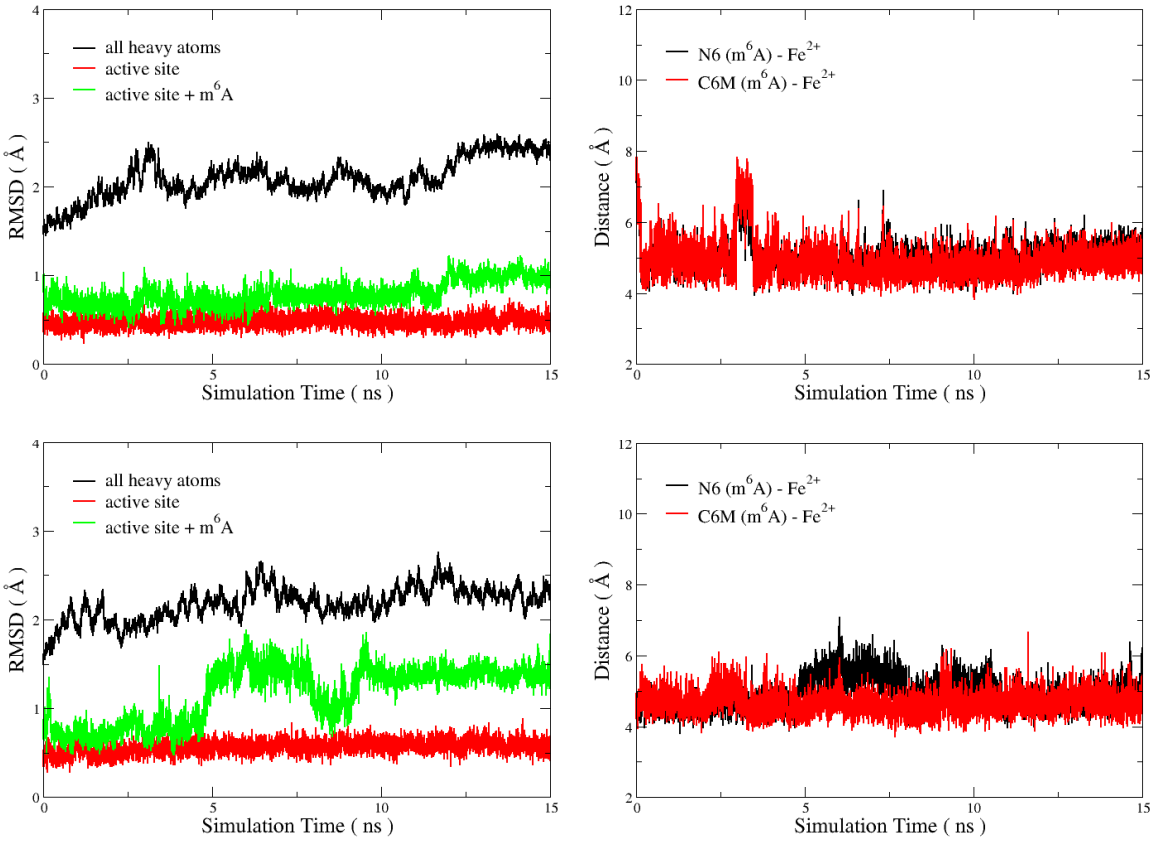

Supplementary Figure S11. RMSD and distances between modified base and Fe^{2+} in equilibrium FTO-m^6A-cry and FTO-m^6A-alkb simulations. m^6A remain stable in the active site, regardless of starting position of the modified base (i.e., "cry" or "alkb").

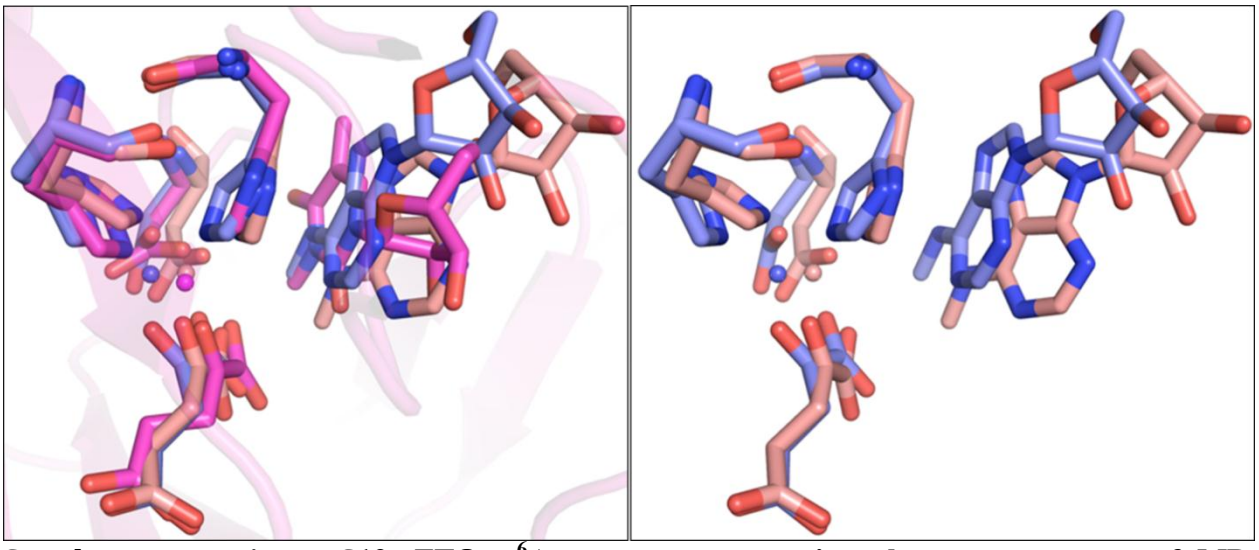

Supplementary Figure S12. FTO-m^{6}A structure comparison between two sets of MD simulations. FTO protein shown in cartoon with active site and modified base highlighted in sticks (FTO crystal structure bind with m^{3}T; FTO-m^{6}A-cry and FTO-m^{6}A-alkb at 10 ns of MD simulation).

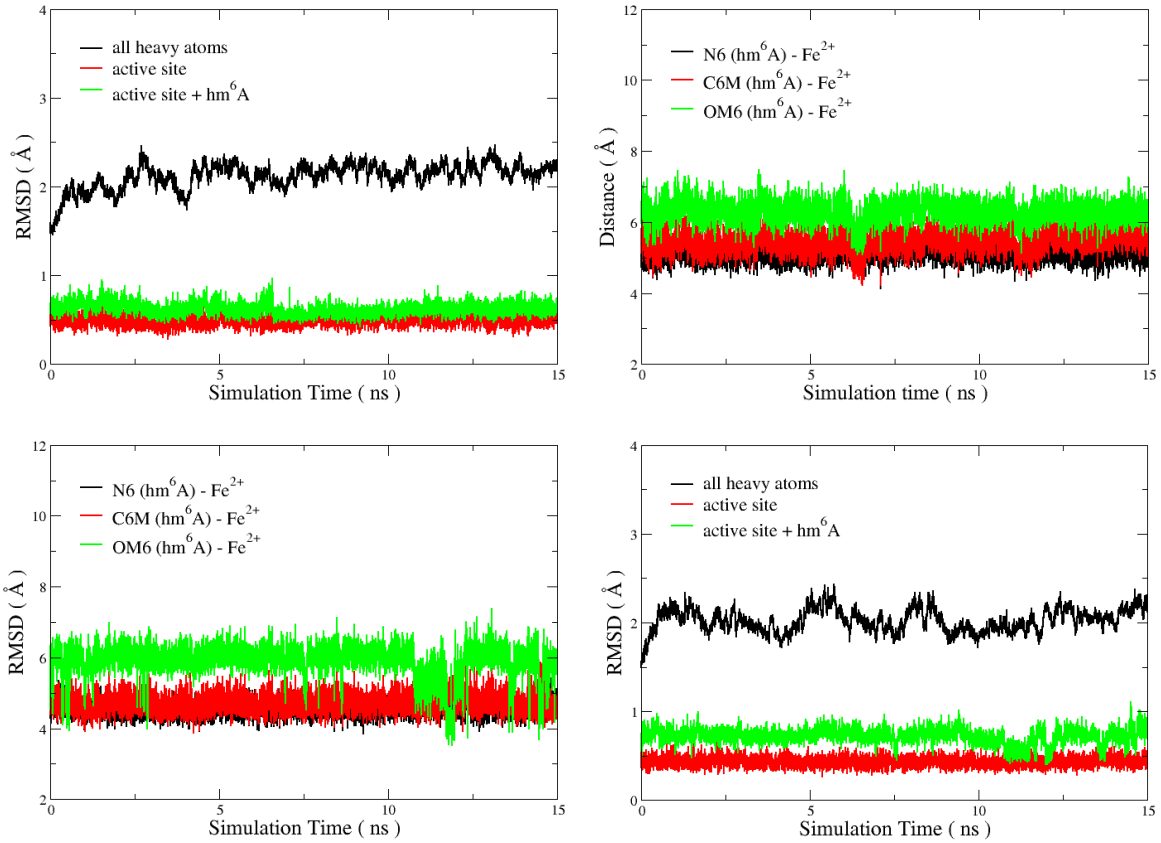

Supplementary Figure S13. RMSD and distances between modified base and Fe^{2+} in equilibrium FTO-hm^{6}A-cry and FTO-hm^{6}A-cry simulations. hm^{6}A remain stable in the active site, regardless of starting position of the modified base (i.e., "cry" or "alkb").

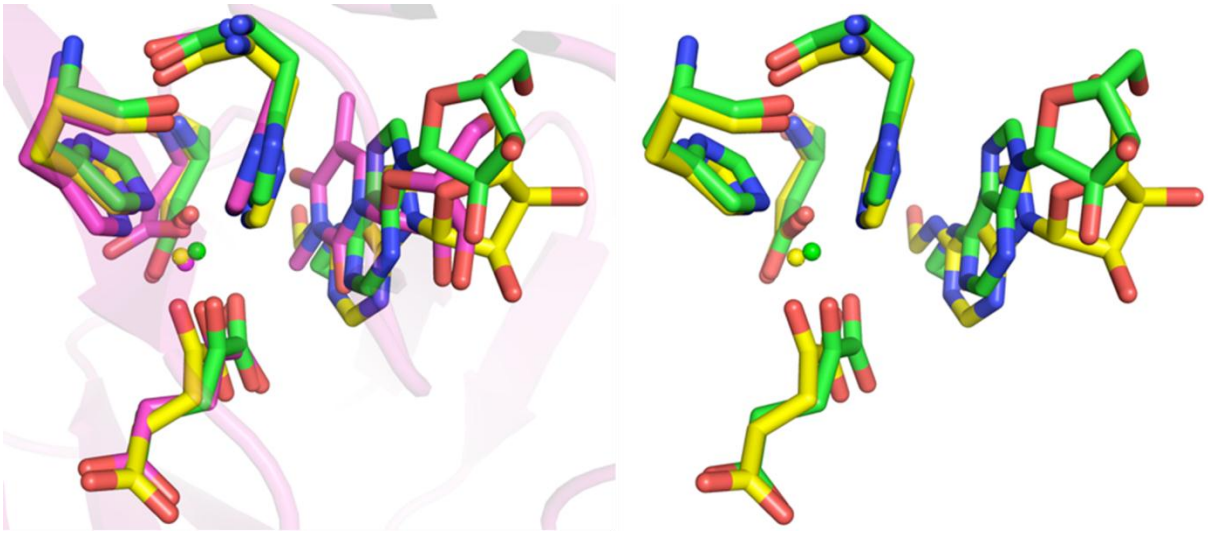

Supplementary Figure S14. FTO-hm^{6}A structure comparison between two sets of MD simulations. FTO protein shown in cartoon with active site and modified base highlighted in sticks (FTO crystal structure bind with m^{3}T; FTO-hm^{6}A-cry and FTO-hm^{6}A-alkb at 10 ns MD simulation).

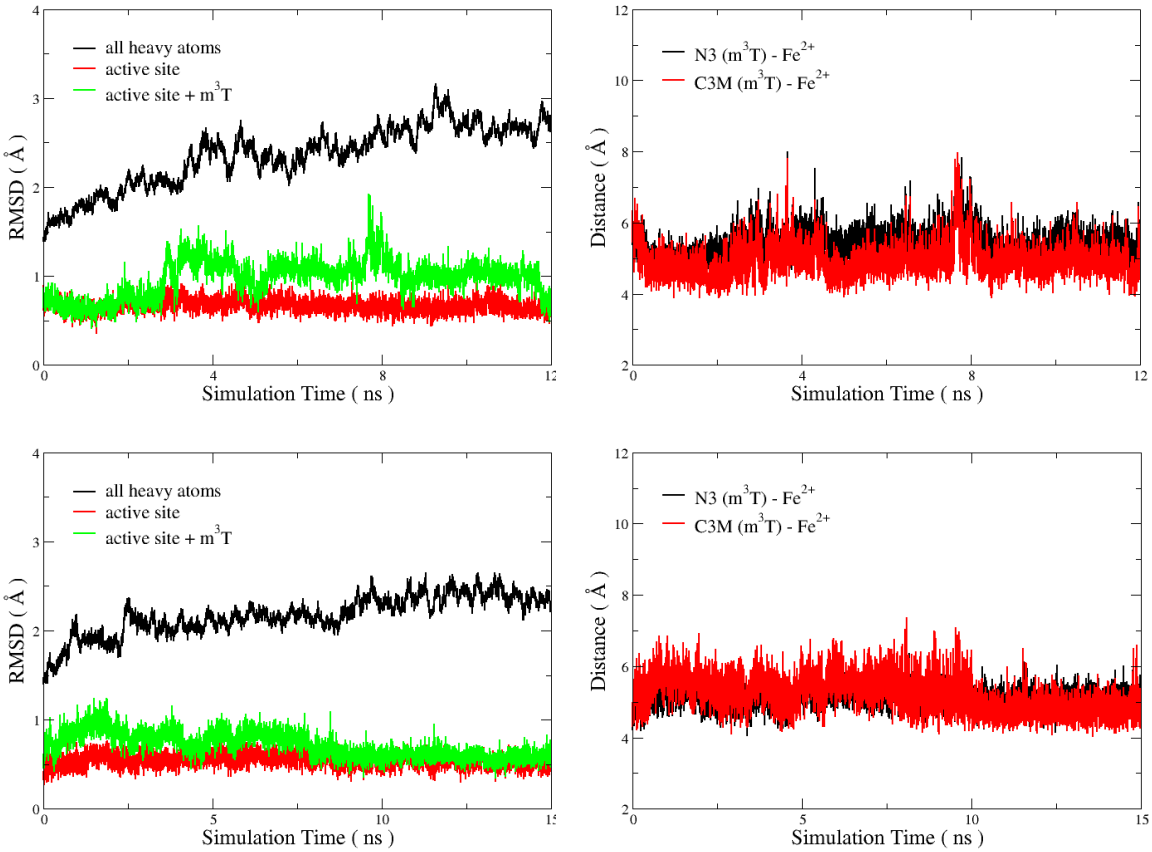

Supplementary Figure S15. RMSD and distances between modified base and Fe^{2+} in equilibrium FTO-m^3T-cry and FTO-m^3T-alkb simulations. m^3T remain stable in the active site, regardless of starting position of the modified base (i.e., "cry" or "alkb").

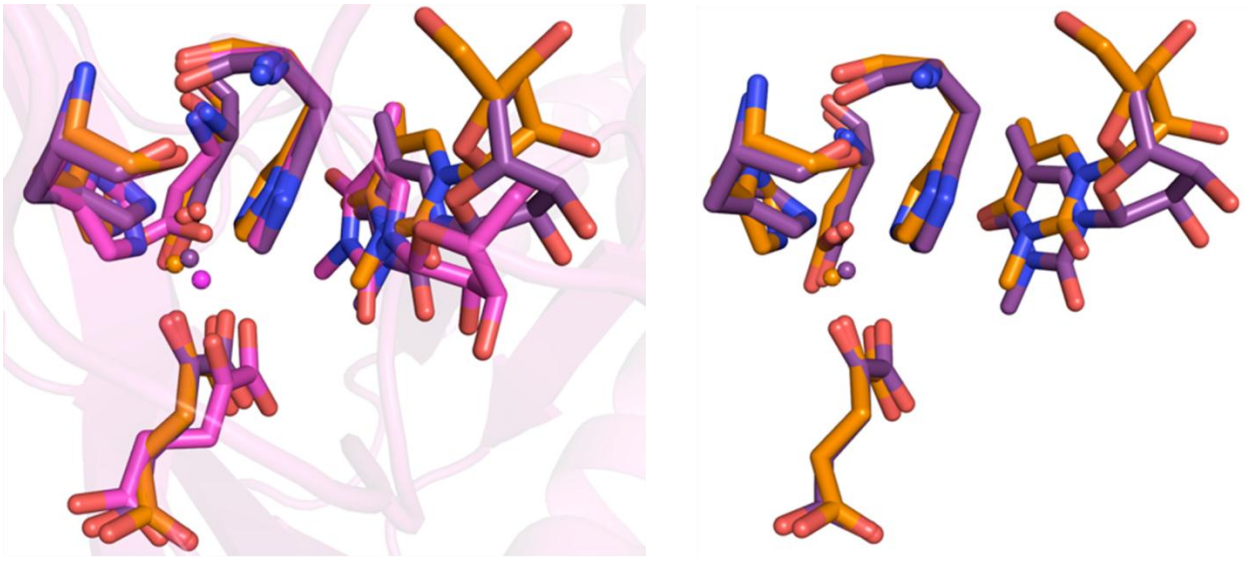

Supplementary Figure S16. FTO-m^{3}T structure comparison between two sets of MD simulations. FTO crystal structure shown in cartoon with active site and modified base in sticks (FTO crystal structure with m^{3}T; FTO-m^{3}T-cry and FTO-m^{3}T-alkb at 10 ns of MD simulation).

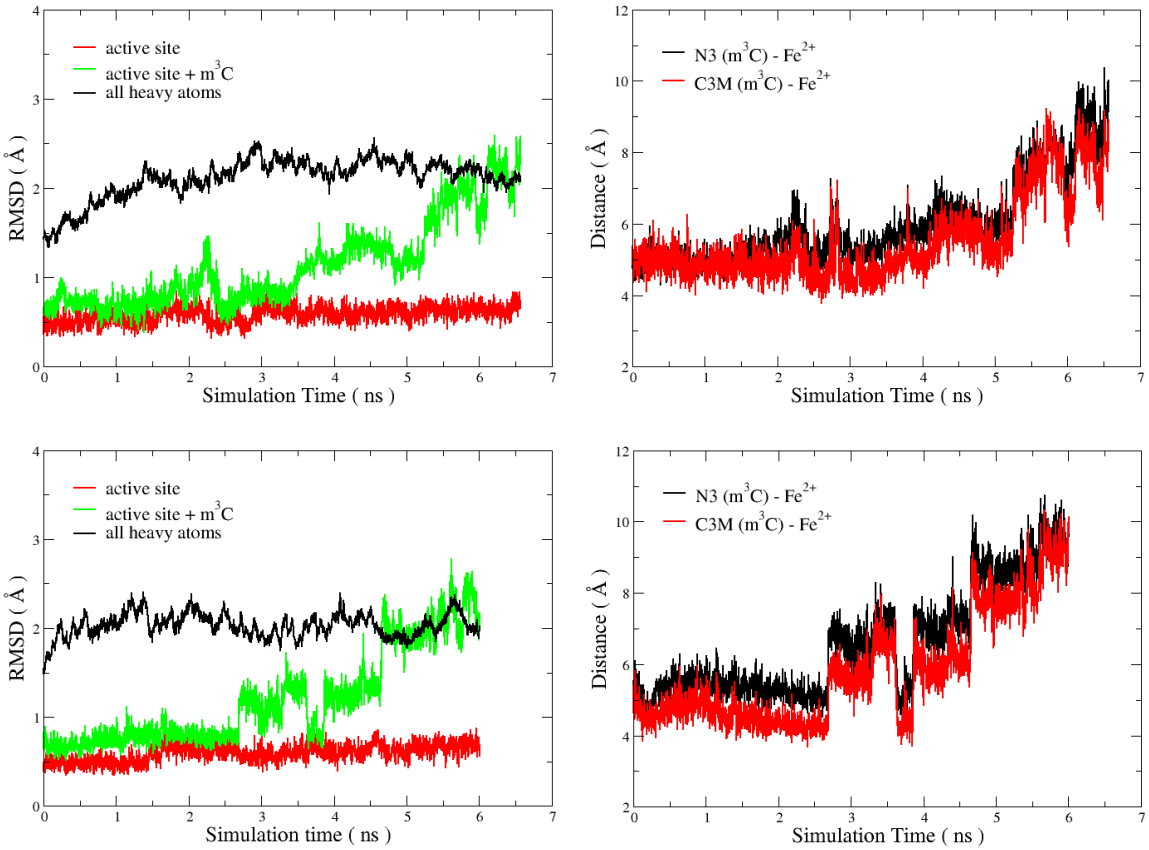

Supplementary Figure S17. RMSD and distances between modified base and Fe^{2+} in equilibrium FTO-m^3C-cry and FTO-m^3C-alkb simulations. Note that m^3C dissociates from the active site after 3ns~5ns. m^3C is NOT stable in FTO, likely due to its positive charge.

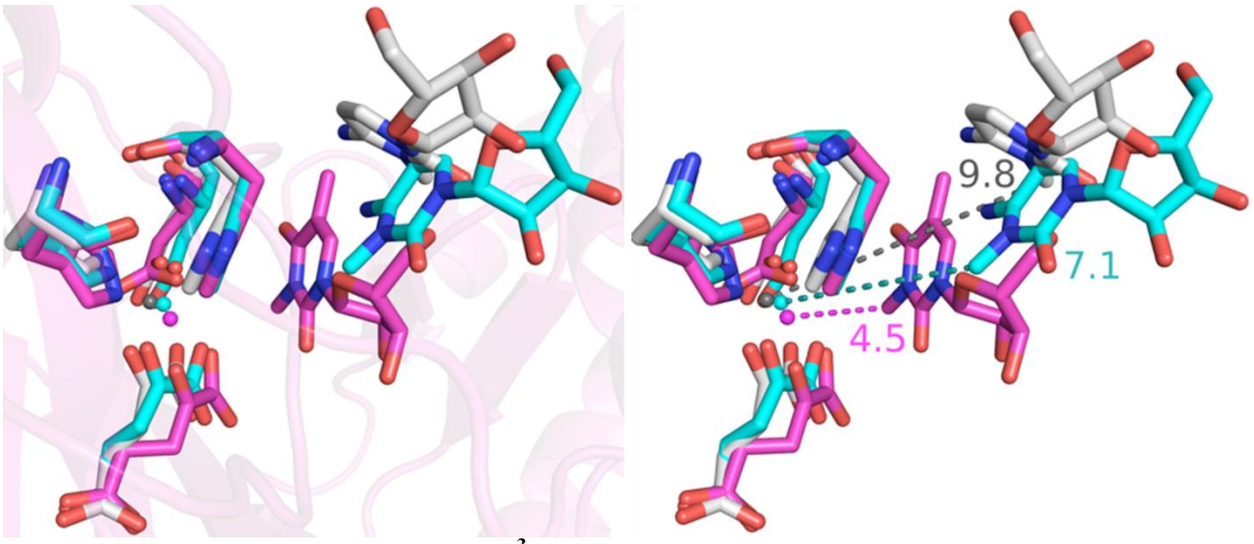

Supplementary Figure S18. FTO-m^{3}C structure comparison between two sets of MD simulations. FTO protein shown in cartoon with active site and modified base in sticks (FTO crystal structure bind with m^{3}T; FTO-m^{3}C-cry and FTO-m^{3}C-alkb at 6 ns of MD simulation). Note that m^{3}C gradually dissociates from the active site.

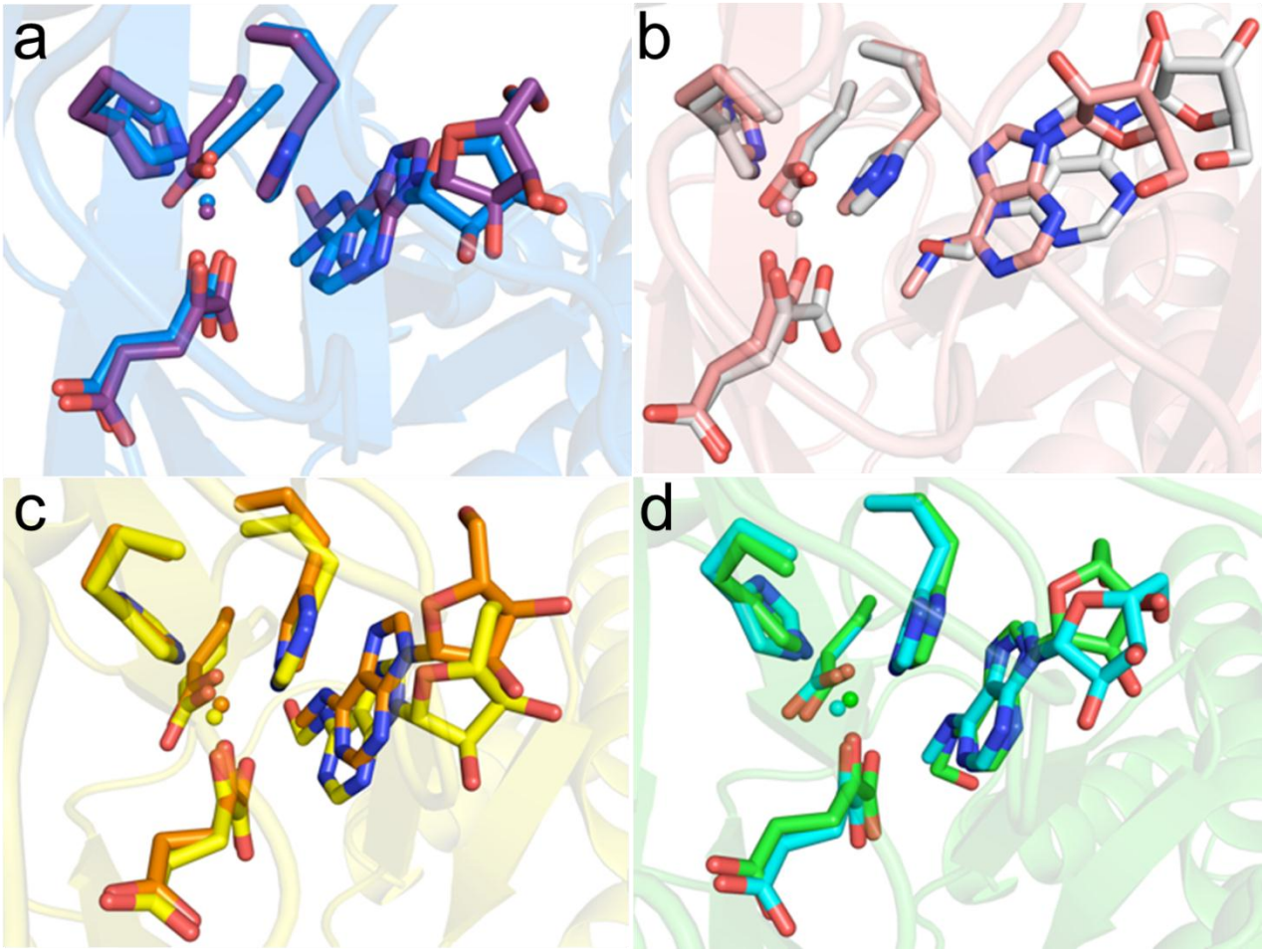

Supplementary Figure S19. Binding mode comparison in different sets of thermodynamic integration simulation. FTO protein shown in cartoon with active site and modified base highlighted in sticks. (**a**) m^6A(FTO-m^6A-cry)→hm^6A, (**b**) m^6A(FTO-m^6A-alkb)→hm^6A, (**c**) hm^6A(FTO-hm^6A-cry)→m^6A, (**d**)hm^6A(FTO-hm^6A-alkb)→ m^6A.

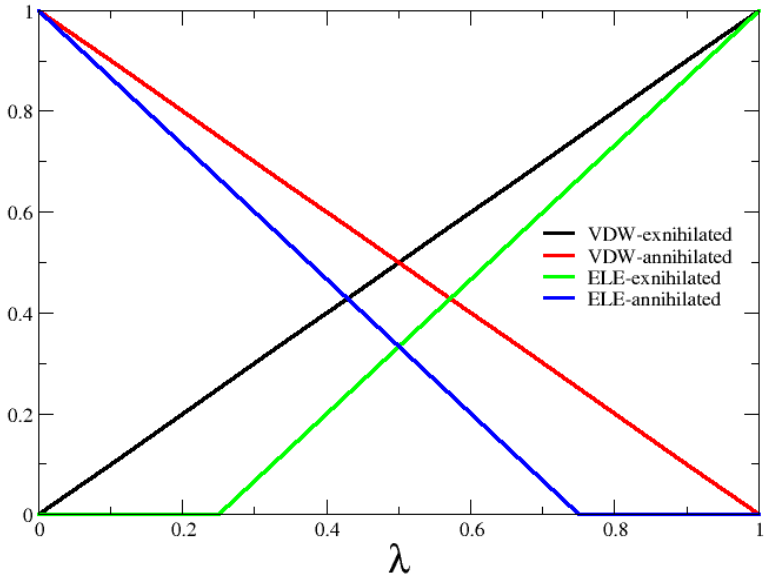

Supplementary Figure S20. Illustration of the coupling schemes for the van der Waals (VDW) and electrostatics (ELE) in the alchemical free energy simulations.

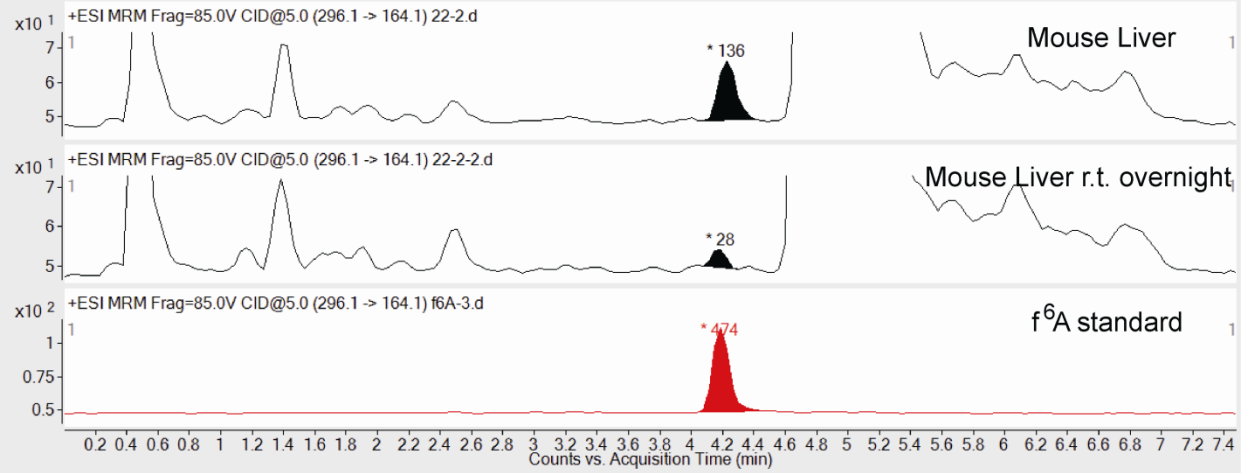

Supplementary Figure S21. Detection and degradation of f^{6}A in mouse liver. f^{6}A can be detected in mouse liver. Signal of f^{6}A decreases upon incubating the digested product overnight at room temperature.

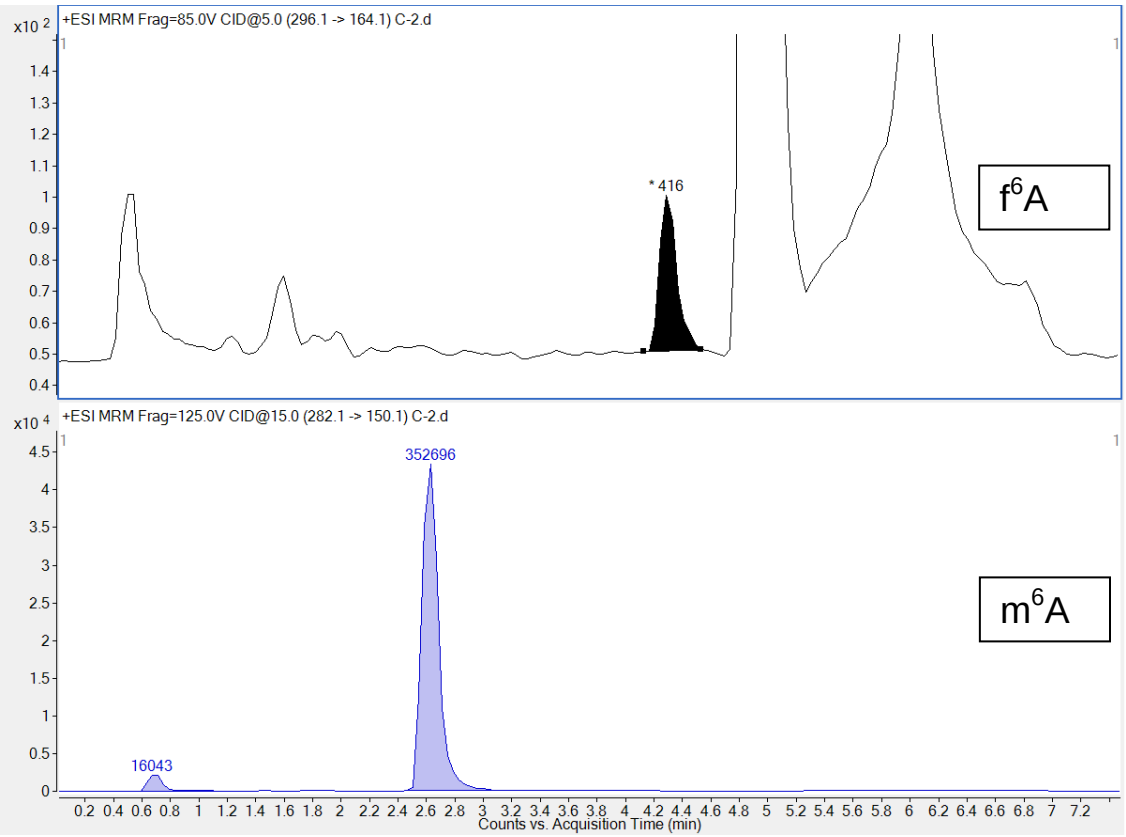

Supplementary Figure S22. Relative amount of f^6A and m^6A in Hela cells. The concentration of the identified f^6A was estimated to be at least 0.5-1% of the total m^6A.

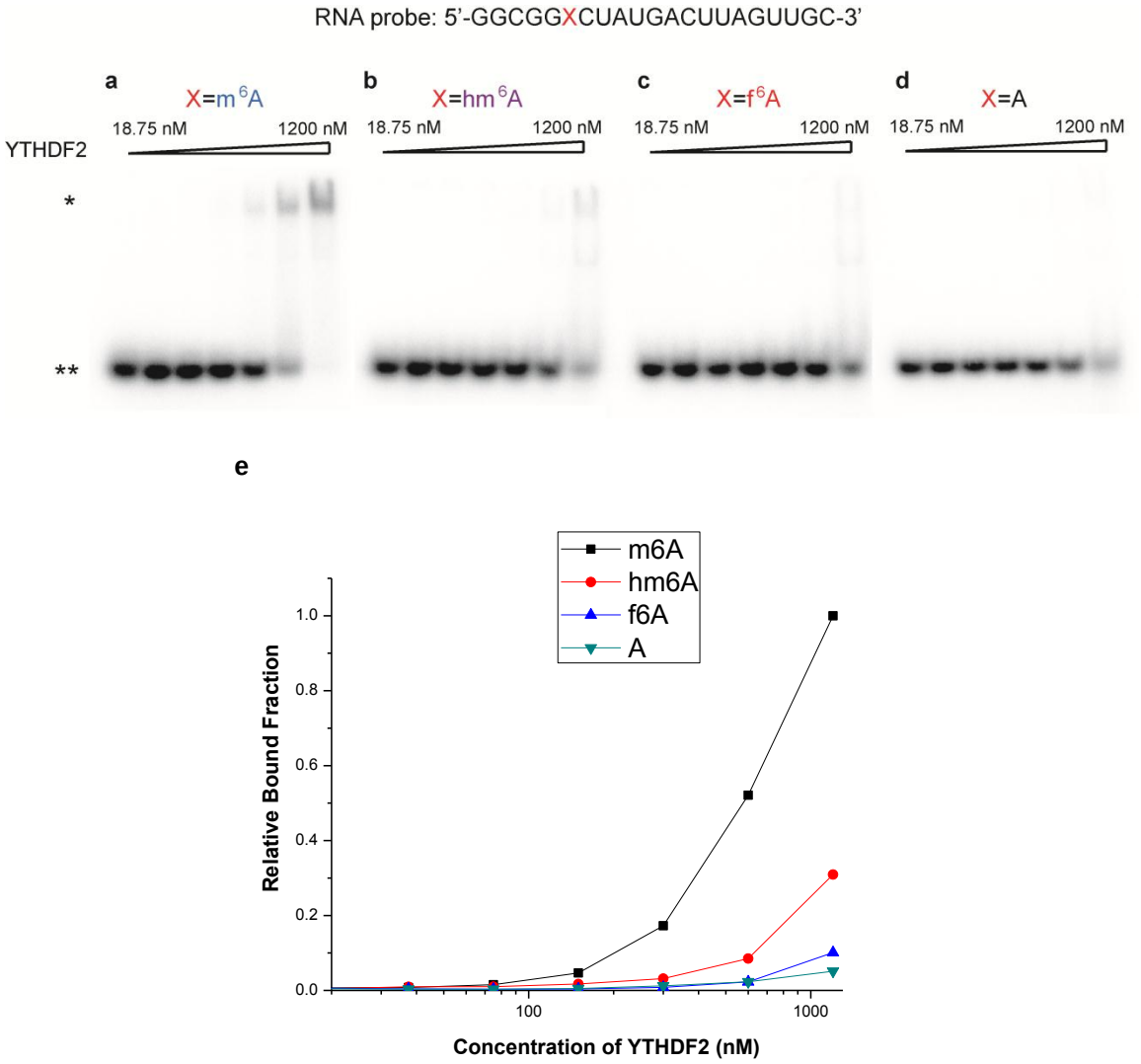

Supplementary Figure S23. EMSA assay of GST-YTHDF2 with RNA containing m^6A, hm^6A, f^6A, and A. hm^6A or f^6A was generated *in situ* by treating m^6A-RNA with 10 uM of FTO for 5 min, or 30 uM of FTO for 20 min at room temperature, respectively. After denaturing FTO, RNA was purified, and mixed with GST-YTHDF2 for 10 min at room temperature. The protein-RNA complex was run in a TBE gel in an ice box for 30 min. The YTHDF2-RNA complex (*) and free RNA probe (**) were labeled. YTHDF2 selectively binds to m^6A with an apparent $K_{d,\,app}$ of 465 ± 16 nM (**a**). The presence of the hm^6A (**b**) and f^6A (**c**) modifications on the same RNA probe led to attenuated binding of YTHDF2 similar to unmethylated A (**d**) with $K_{d,\,app}$ larger than 1.2 uM. (**e**) The intensity of shifted bands in EMSA assay are quantified and plotted vs. the concentration of YTHDF2 protein. The $K_{d,app}$ of YTHDF2 to m^6A is estimated to be 465±16 nM, hm^6A, f^6A, and A-RNA has $K_{d,app}$ larger than 1200 nM.

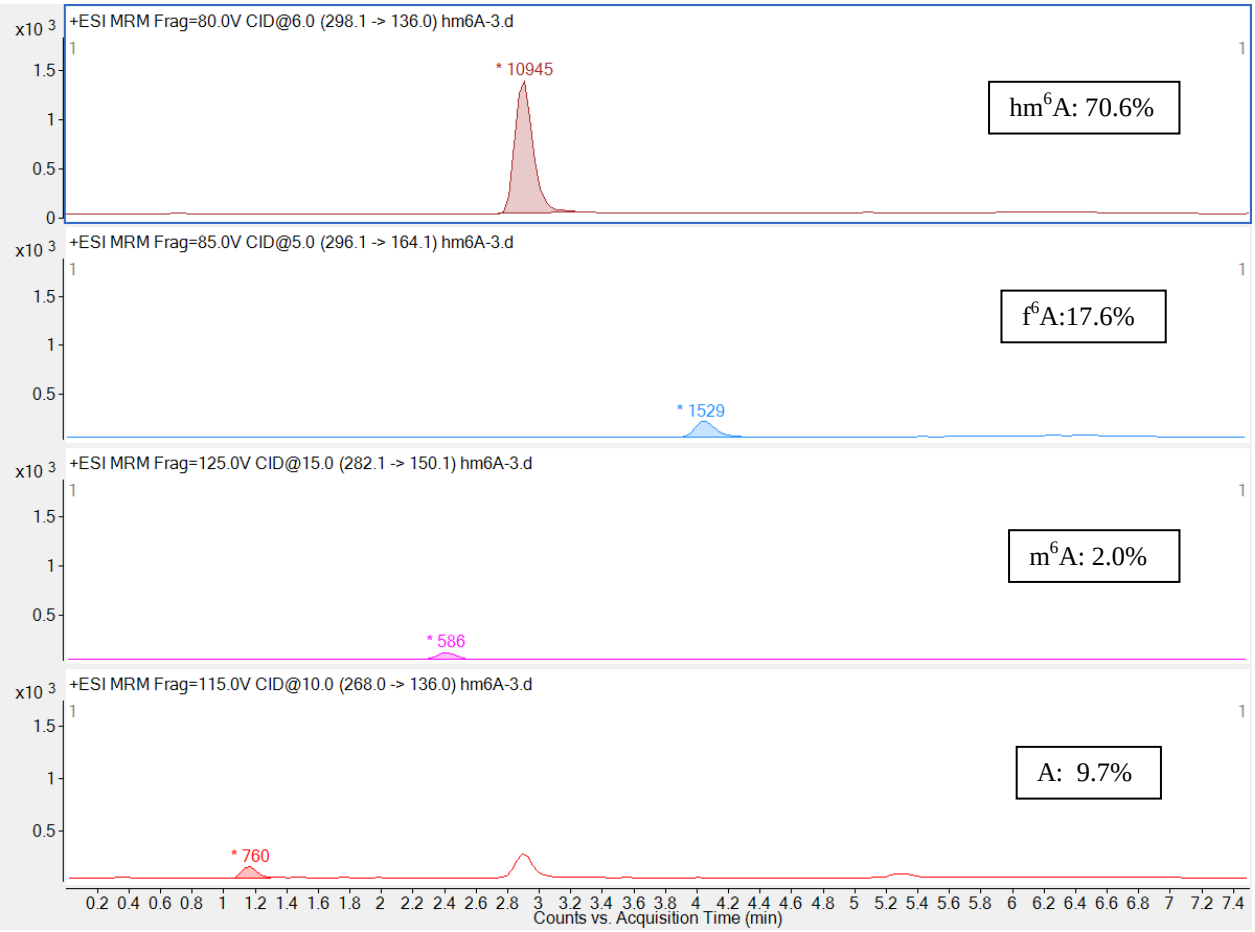

Supplementary Figure S24. Composition of X in hm^{6}A-RNA for YTHDF2 EMSA assay. hm^{6}A composites about 70% in modified RNA used in EMSA assay.

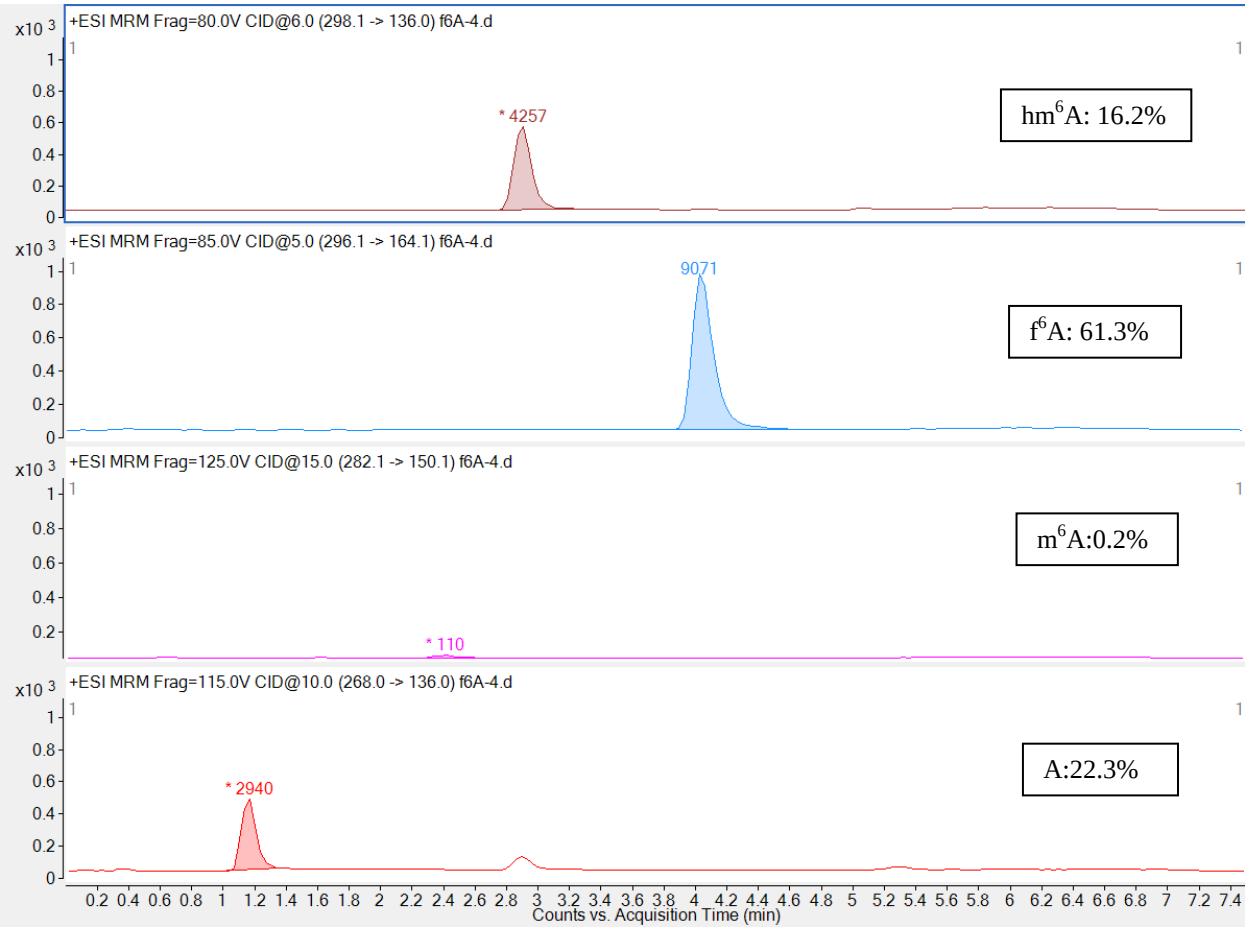

Supplementary Figure S25. Composition of X in f^{6}A-RNA for YTHDF2 EMSA assay. f^{6}A composites about 60% in modified RNA used in EMSA assay.

Supplementary Table S1. Relative binding free energies of m^6A and hm^6A from alchemical free energy simulations.

TI direction	Initial coordinates	ΔG in protein (kcal/mol)	ΔG in water (kcal/mol)	ΔΔG binding (kcal/mol)
m^6A to hm^6A (2ns)	FTO-m^6A-cry	-10.0 (0.5)	-9.6 (0.2)	-0.4 (0.5)
m^6A to hm^6A (2ns)	FTO-m^6A-alkb	-10.7 (0.4)	-9.6 (0.2)	-1.1 (0.4)
hm^6A to m^6A (2ns)	FTO-hm^6A-cry	12.5 (0.3)	9.7 (0.2)	2.8 (0.4)
hm^6A to m^6A(1.6ns)	FTO-hm^6A-alkb	11.5 (0.4)	9.7 (0.1)	1.8 (0.4)

All independent simulations predict a slightly stronger binding (ranging from 0.4 to 2.8 kcal/mol) for hm^6A than m^6A (they have different signs in the first and second two rows because the alchemical simulations are done in different directions). Values in parentheses are statistical uncertainties.

Supplementary Methods

Synthesis procedure of N^6-hydroxymethyladenosine (hm^6A) (Supplementary Figure S2a). 100 uM of Adenosine (**1**) was treated with 30 mM of formaldehyde at 60 ºC for 4 h. The mixture was diluted with water and analyzed by HPLC (200 times dilution) and HPLC-MS/MS (1,000 times dilution) to confirm the production of hm^6A (**2**). N^6-methylene-adenosine (**3**) co-exists in equilibration with hm^6A as a dehydration product. hm^6A and N^6-methylene-adenosine was characterized by HPLC-MS/MS. hm^6A has a MS/MS transition of 298.1 to 136.0; N^6-methylene-adenosine has a MS/MS transition of 280.0 to 136.0.

Synthesis procedure of N^6-formyladenosine (f^6A) (Supplementary Figure S2b). For the preparation of **4**, 2 g of adenosine (**1**, 7.5 mmol) was mixed with 4.5 g of TBDMSCl (30 mmol), and 3.1 g of imidazole (45 mmol) in 40 mL of DMF. The mixture was stirred at r. t. overnight, DMF was evaporated; the residue was washed with water once. Loaded on silica chromatography, the product was eluted with hexane/EtOAc (2:1 to 1:1) with 95% yield. **4** was mixed with 3.0 equiv. of dimethyl acetal-DMF in dry MeOH, stirred at 40 ºC for 3 h. **6** was isolated with silica chromatography by hexane/EtOAc (5:1 to 3:1) with a yield of 80%. 70 mg of **6** was treated with 0.3 equiv of $HOBt\cdot H_2O$ in 1 mL of dry MeOH at 0 ºC for 1 h, and **7** was isolated by silica chromatography using hexane/EtOAc (10:1 to 5:1) with a yield of 30%, **7** was treated with 10.0 equiv of $HF\cdot NEt_3$ and 10.0 equiv of pyridine in THF at r.t. for 4 h, dried under vacuum, and subjected to silica chromatography using CH_2Cl_2/MeOH (20:1 to 4:1) to give N^6-formyladenosine (**8**) with a yield of 50%. **8** was dissolved in DMSO, and stored at -78 ºC. d_6-DMSO is used as the solvent for NMR analysis. ^{1}H NMR (DMSO-d_6, 500MHz) δ11.395 (br, 1H), 9.953 (s, 1H), 8.766 (s, 1H), 8.617 (s, 1H), 6.034 (d, 1H, *J*=5.5 Hz), 5.574 (d, 1H, *J*=6.0 Hz), 5.278 (d, 1H, *J*=5.0 Hz), 5.185 (t, 1H, *J*=5.5 Hz), 4.625 (dd, 1H, *J*=5.5, 5.5 Hz), 4.202 (dd, 1H, *J*=5.0, 4.0 Hz), 4.001 (dd, 1H, *J*=3.5, 4.0 Hz) 3.713 (m, 1H), 3.607 (m, 1H) ppm; ^{13}C NMR (DMSO-d_6, 125MHz) δ165.193, 152.995, 152.649, 150.665, 144.237, 122.245, 88.690, 86.697, 74.769, 71.239, 62.204 ppm. UV/Vis: λ_{max} 274 nm, $\varepsilon_{260nm} = 1.30\times10^4\ M^{-1}cm^{-1}$, $\varepsilon_{max(274nm)} = 1.83\times10^4\ M^{-1}cm^{-1}$, LC-QQQ-MS/MS (Positive): $[M+H]^+$ = 296.1, $[Base+H]^+$ = 164.0, HRMS (m/z) for $C_{11}H_{13}N_5O_5$: $[MH]^+$ = 296.0995(calcd.), 296.1009 (found).

Electrophoretic mobility shift assay (EMSA) of modified RNA with YTHDF2 protein. Full-length human YTHDF2 was cloned into pGEX-4T-1, expressed in *E. coli* BL21 (DE3), and purified by GST-affinity column, and MonoS. 20 pmol of m^6A-RNA was labeled by 3 uL of [γ-^{32}P]ATP (6000 Ci/mmol; Perkin-Elmer) in 20 uL of reaction buffer by 20 units of T4 polynucleotide kinase (Fermentas). After addition of 15 uL of H_2O, the labeled RNA was cleaned up using phenol-$CHCl_3$ extraction. SP-6 spin column, Fe, α-KG, KCl, and ascorbic acid were added together with FTO at room temperature for defined time (10 uM, 5 min for generating hm^6A; 30 uM, 20 min for generating f^6A.). 2 mM of EDTA and 100 mM of Guanidine thiocyanate (pH 6.7) were added to quench the reaction. The reaction mixture was frozen-thawed three times between liquid nitrogen and 37 ºC in order to completely denature FTO protein. The solution was cleaned up again using phenol-$CHCl_3$ extraction through SP-6 spin column. The flow through was diluted 10 times; 1 uL of this labeled RNA was used in the EMSA assay. 1 uL of the labeled RNA was mixed with 2.5 uL of protein in a series of two-fold

dilution, and 6.5 uL of EMSA buffer (10 mM of HEPES, pH 8.0, 50 mM of KCl, 1mM of EDTA, 0.05% of Triton X-100, 5% of glycerol, 10 ug/mL of Salmon DNA). The mixture was incubated at room temperature for 10 min, and on ice for 10 min. 0.5 uL of Novex® Hi-Density TBE Sample Buffer (Invitrogen) was added before loading to a Novex® 4-12% TBE gel. The gel was run with 0.5× TBE at 200 V for 30 min in an ice box. After drying, the gel was exposed to a storage phosphor screen (K-Screen; Fuji film) and quantified through Bio-Rad Molecular Imager FX in combination with Quantity One software (Bio-Rad). The intensity of shifted RNA-protein complex is quantified.

Two independent protocols for setting up the FTO-base systems. The initial coordinates were taken from the crystal structure of FTO bound with Fe^{2+}, *N*-oxalyglycine and m^3T (PDB ID: 3LFM). We replaced the N-oxalyglycine (antagonist of FTO) with the active co-factor 2-ketoglutarate (2KG). The coordinates of the modified bases were generated in two different ways, and two independent sets of simulations were carried out accordingly. The first approach is to fix the sugar ring position of m^3T in 3LFM, and then mutate the original m^3T to m^3C, m^6A or hm^6A, respectively. These systems are labeled as FTO-m^3T-cry, FTO-m^3C-cry, FTO-m^6A-cry and FTO-hm^6A-cry, respectively. The second protocol is to align the AlkB-DNA complex crystal structures with FTO based on 3D protein structure similarity calculated with the Protein Comparison Tool[35] and then take the coordinates of the modified bases from the aligned AlkB complexes. We use PDB file 3O1O to derive the coordinates for m^3T, 3O1Mfor m^3C, and 3O1Pfor εA; εA is then mutated to m^6A or hm^6A. These systems are labeled as FTO-m^3T-alkb, FTO-m^3C-alkb, FTO-m^6A-alkb and FTO-hm^6A-alkb, respectively.

MD simulation setup. Hydrogen atoms of the FTO protein and modified bases were added with HBUILD[36] in CHARMM, and all basic and acidic amino acids were kept in their physiological protonation states. Each of the protein-base complexes was solvated by a pre-equilibrated cubic water box with the box length of 119 Å. 50 mM NaCl was added to the system and around 161,000 atoms were included in each simulation. The protein atoms are described with the CHARMM22 all-atom force field for protein;[37] the modified bases are described with a modified CHARMM27 all-hydrogen nucleic acids force field;[38,39] water molecules are described with the TIP3P model.[40] The iron center is described with a simple molecular mechanical model we have developed recently for the AlkB protein family. In the FTO crystal structure, an antagonist (N-oxalyglycine) is bound to the active site, and the distances between Fe^{2+} and its coordinating ligands are rather different from other proteins in the AlkB family (**Supplementary Figure S19**); the latter is likely due to antagonist binding as well as the lower resolution of the FTO crystal structure (I think the antagonist binding also plays a role). Therefore, the prepared FTO-modified systems were gradually relaxed with careful minimization with CHARMM[41] before MD simulations.

All MD simulations were carried out with the NAMD2.8 program[42] with standard periodic boundary conditions. The systems were relaxed with 2000 steps energy minimization under the constrain of 10 kcal/(mol·Å^2), 5 kcal/(mol·Å^2), 1 kcal/(mol·Å^2) and 0 kcal/(mol·Å^2) on the heavy atoms, respectively; then gradually equilibrated at 300 K for 300 ps using the NVT ensemble and a damping coefficient of 5.0 ps^{-1}. Further equilibration and production runs were carried out using the NPT ensemble, with the pressure set to 1.01325 bar. Covalent bonds involving hydrogen were restrained with the SHAKE algorithm.[43] Lennard-Jones interactions

were switched off gradually from 10 Å to 12 Å with a switching function. Electrostatic interactions were treated with the particle mesh Ewald (PME) scheme,[44] and the grid size was 120^3. A time step of 1.0 fs was used throughout the simulation.

Alchemical free energy simulations for relative binding affinities. Alchemical free energy simulations with the thermodynamic integration (TI) algorithm[45] was used to calculate the relative binding affinity of m^6A and hm^6A to FTO. The initial coordinates of the alchemical free energy simulations were taken from the MD simulations by the end of 10ns. Independent TI simulations in opposite directions (i.e., mutating m^6A to hm^6A or hm^6A to m^6A) were carried out in both FTO and water with the NAMD2.8 package. The dual topology protocol[46] and recommended coupling schemes for electrostatic and van der Waals (VDW) interactions described in NAMD2.8 were used. For all TI simulations, a softcore VDW radius shifting[47,48] coefficient of 4.0 was used. As shown in **Supplementary Figure S20**, the VDW interactions involving exnihilated particle were fully decoupled at $\lambda=0$, completely coupled at $\lambda=1$, and linearly turned on from $\lambda=0$ to $\lambda=1$; the VDW interactions involving annihilated particles were completely coupled at $\lambda=0$, fully decoupled at $\lambda=1$, and linearly turned off from $\lambda=0$ to $\lambda=1$. A somewhat different coupling scheme was used to treat the electrostatic interactions: the exnihilated particles were fully decoupled for $\lambda\subseteq(0, 0.25)$, completely coupled at $\lambda=1$, and linearly turned on from $\lambda=0.25$ to $\lambda=1$; for the annihilated particles, electrostatics were completely coupled at $\lambda=0$, fully decoupled for $\lambda \geq 0.75$, and linearly turned off from $\lambda=0$ to $\lambda=0.75$. To avoid end-point catastrophes in certain windows while mutating m^6A to hm^6A in the FTO-alkb setup, we adjusted the way of treating electrostatic interactions: electrostatic interactions for the exnihilated particles were fully decoupled for $\lambda\subseteq(0, 0.5)$ and completely coupled at $\lambda=1$; for the annihilated particles, electrostatics were completely coupled at $\lambda=0$, and fully decoupled for $\lambda \geq 0.5$.

For the TI simulations in water, a $\Delta\lambda=0.05$ was used and with 21 windows in total. We took the base structures from MD simulations of FTO-m^6A-cry, FTO-hm^6A-cry, FTO-m^6A-alkb or FTO-hm^6A-alkb by the end of 10ns, and solvated them with a 35 Å water box. Then, for each of the four sets of simulations, a 500 ps equilibration with dual topology at $\lambda=0$ was carried out, so as to generate the initial coordinates for the $\lambda=0$ window. For each window of the TI simulations, 20 ps equilibration and 100 ps production run was carried out, and the final coordinates of the simulation were used as the starting structure for the next window. We then continued TI simulations with another 400 ps production run for each window. (We run a shorter simulation 100 ps to generate the coordinate for the next window, and continue the simulation with another 400 ps production run in each window.) For the mutations in protein, a $\Delta\lambda=0.05$ was used near the two ends (0, 1) and $\Delta\lambda=0.1$ was used in the middle; 13 windows were used for the mutation from m^6A to h^6A in FTO-alkb, while 15 windows were used in the other three simulations. To generate the initial coordinates for the $\lambda=0$ window, we took the snapshot after 10ns MD simulation of FTO-m^6A-cry, FTO-hm^6A-cry, FTO-m^6A-alkb or FTO-hm^6A-alkb, and then carried out 500ps of equilibration with dual topology at $\lambda=0$. After the initial coordinates for all windows were generated with the same as way described above, another 400 ps of equilibration and 1.2 to 1.6 ns production run were carried out for each window.

YTHDF2 Nucleotide Sequence (Isoform 2 CDS 1590 nt):
ATGTCAGATTCCTACTTACCCAGTTACTACAGTCCCTCCATTGGCTTCTCCTATTCTTTGGGTGAA

GCTGCTTGGTCTACGGGGGGTGACACAGCCATGCCCTACTTAACTTCTTATGGACAGCTGAGCAA
CGGAGAGCCCCACTTCCTACCAGATGCAATGTTTGGGCAACCAGGAGCCCTAGGTAGCACTCCAT
TTCTTGGTCAGCATGGTTTTAATTTCTTTCCCAGTGGGATTGACTTCTCAGCATGGGGAAATAACA
GTTCTCAGGGACAGTCTACTCAGAGCTCTGGATATAGTAGCAATTATGCTTATGCACCTAGCTCC
TTAGGTGGAGCCATGATTGATGGACAGTCAGCTTTTGCCAATGAGACCCTCAATAAGGCTCCTGG
CATGAATACTATAGACCAAGGGATGGCAGCACTGAAGTTGGGTAGCACAGAAGTTGCAAGCAAT
GTTCCAAAAGTTGTAGGTTCTGCTGTTGGTAGCGGGTCCATTACTAGTAACATCGTGGCTTCCAAT
AGTTTGCCTCCAGCCACCATTGCTCCTCCAAAACCAGCATCTTGGGCTGATATTGCTAGCAAGCC
TGCAAAACAGCAACCTAAACTGAAGACCAAGAATGGCATTGCAGGGTCAAGTCTTCCGCCACCC
CCGATAAAGCATAACATGGATATTGGAACTTGGGATAACAAGGGTCCCGTTGCAAAAGCCCCCT
CACAGGCTTTGGTTCAGAATATAGGTCAGCCAACCCAGGGGTCTCCTCAGCCTGTAGGTCAGCAG
GCTAACAATAGCCCACCAGTGGCTCAGGCATCAGTAGGGCAACAGACACAGCCATTGCCTCCAC
CTCCACCACAGCCTGCCCAGCTTTCAGTCCAGCAACAGGCAGCTCAGCCAACCCGCTGGGTAGCA
CCTCGGAACCGTGGCAGTGGGTTCGGTCATAATGGGGTGGATGGTAATGGAGTAGGACAGTCTC
AGGCTGGTTCTGGATCTACTCCTTCAGAACCCCACCCAGTGTTGGAGAAGCTTCGGTCCATTAAT
AACTATAACCCCAAAGATTTTGACTGGAATCTGAAACATGGCCGGGTTTTCATCATTAAGAGCTA
CTCTGAGGACGATATTCACCGTTCCATTAAGTATAATATTTGGTGCAGCACAGAGCATGGTAACA
AGAGACTGGATGCTGCTTATCGTTCCATGAACGGGAAAGGCCCCGTTTACTTACTTTTCAGTGTC
AACGGCAGTGGACACTTCTGTGGCGTGGCAGAAATGAAATCTGCTGTGGACTACAACACATGTG
CAGGTGTGTGGTCCCAGGACAAATGGAAGGGTCGTTTTGATGTCAGGTGGATTTTTGTGAAGGAC
GTTCCCAATAGCCAACTGCGACACATTCGCCTAGAGAACAACGAGAATAAACCAGTGACCAACT
CTAGGGACACTCAGGAAGTGCCTCTGGAAAAGGCTAAGCAGGTGTTGAAAATTATAGCCAGCTA
CAAGCACACCACTTCCATTTTTGATGACTTCTCACACTATGAGAAACGCCAAGAGGAAGAAGAA
AGTGTTAAAAAGGAACGTCAAGGTCGTGGGAAATAA

Cloning Primer for human YTHDF2

Forward: 5'-CGTACGGATCCATGTCAGATTCCTACTTACCCAG-3'BamH1 site

Reverse: 5'-CGTCAAGGTCGTGGGAAATGACTCGAGCCTAAG-3' Xho1 site

Supplementary References:

35. Prlic, A. et al. Pre-calculated protein structure alignments at the RCSB PDB website. *Bioinformatics* **26**, 2983-2985 (2010).
36. Brunger, A.T. & Karplus, M. Polar Hydrogen Positions in Proteins - Empirical Energy Placement and Neutron-Diffraction Comparison. *Proteins-Structure Function and Genetics* **4**, 148-156 (1988).
37. MacKerell, A.D. et al. All-atom empirical potential for molecular modeling and dynamics studies of proteins. *Journal of Physical Chemistry B* **102**, 3586-3616 (1998).
38. Foloppe, N. & MacKerell, A.D. All-atom empirical force field for nucleic acids: I. Parameter optimization based on small molecule and condensed phase macromolecular target data. *Journal of Computational Chemistry* **21**, 86-104 (2000).
39. MacKerell, A.D. & Banavali, N.K. All-atom empirical force field for nucleic acids: II. Application to molecular dynamics simulations of DNA and RNA in solution. *Journal of Computational Chemistry* **21**, 105-120 (2000).

40. Jorgensen, W.L., Chandrasekhar, J., Madura, J.D., Impey, R.W. & Klein, M.L. Comparison of Simple Potential Functions for Simulating Liquid Water. *Journal of Chemical Physics* **79**, 926-935 (1983).
41. Brooks, B.R. et al. Charmm - a Program for Macromolecular Energy, Minimization, and Dynamics Calculations. *Journal of Computational Chemistry* **4**, 187-217 (1983).
42. Phillips, J.C. et al. Scalable molecular dynamics with NAMD. *Journal of Computational Chemistry* **26**, 1781-1802 (2005).
43. Ryckaert, J.P., Ciccotti, G. & Berendsen, H.J.C. Numerical-Integration of Cartesian Equations of Motion of a System with Constraints - Molecular-Dynamics of N-Alkanes. *Journal of Computational Physics* **23**, 327-341 (1977).
44. Essmann, U. et al. A Smooth Particle Mesh Ewald Method. *Journal of Chemical Physics* **103**, 8577-8593 (1995).
45. Straatsma, T.P. & Mccammon, J.A. Multiconfiguration Thermodynamic Integration. *Journal of Chemical Physics* **95**, 1175-1188 (1991).
46. Gao, J., Kuczera, K., Tidor, B. & Karplus, M. Hidden Thermodynamics of Mutant Proteins - a Molecular-Dynamics Analysis. *Science* **244**, 1069-1072 (1989).
47. Zacharias, M., Straatsma, T.P. & Mccammon, J.A. Separation-Shifted Scaling, a New Scaling Method for Lennard-Jones Interactions in Thermodynamic Integration. *Journal of Chemical Physics* **100**, 9025-9031 (1994).
48. Beutler, T.C., Mark, A.E., Vanschaik, R.C., Gerber, P.R. & Vangunsteren, W.F. Avoiding Singularities and Numerical Instabilities in Free-Energy Calculations Based on Molecular Simulations. *Chemical Physics Letters* **222**, 529-539 (1994).